Noninvasive localized delivery of Herceptin to the mouse brain by MRI-guided focused ultrasound-induced blood–brain barrier disruption

Manabu Kinoshita, Nathan McDannold, Ferenc A. Jolesz, and Kullervo Hynynen*

Department of Radiology, Brigham and Women's Hospital, and Harvard Medical School, 75 Francis Street, Boston, MA 02115

Communicated by Floyd Dunn, University of Illinois at Urbana–Champaign, Urbana, IL, May 24, 2006 (received for review February 15, 2006)

Antibody-based anticancer agents are promising chemotherapeutic agents. Among these agents, Herceptin (trastuzumab), a humanized anti-human epidermal growth factor receptor 2 (HER2/c-erbB2) monoclonal antibody, has been used successfully in patients with breast cancer. However, in patients with brain metastasis, the blood–brain barrier limits its use, and a different delivery method is needed to treat these patients. Here, we report that Herceptin can be delivered locally and noninvasively into the mouse central nervous system through the blood–brain barrier under image guidance by using an MRI-guided focused ultrasound blood–brain barrier disruption technique. The amount of Herceptin delivered to the target tissue was correlated with the extent of the MRI-monitored barrier opening, making it possible to estimate indirectly the amount of Herceptin delivered. Histological changes attributable to this procedure were minimal. This method may represent a powerful technique for the delivery of macromolecular agents such as antibodies to treat patients with diseases of the central nervous system.

brain tumor | microbubble

Advances in tumor cell biology have led to the availability of new types of anticancer chemotherapeutic agents that are superior to the conventional agents in that they can precisely target the signal-transduction system unique to malignant tumor cells, thereby lowering the toxic effects of anticancer agents on normal cells. Herceptin (trastuzumab; Genentech) is a humanized mAb that targets human epidermal growth factor receptor 2 (HER2/c-erbB2) expressed in breast cancer cells. It has been used to treat breast cancer patients, and it has succeeded remarkably in controlling local and distal breast cancer lesions (1). Although breast cancer often metastasizes to the brain (2), Herceptin could only be used to treat extracranial lesions because there is currently no efficient method to deliver it to the CNS. The increased use of Herceptin to treat breast cancer patients has resulted in a higher incidence of brain metastasis from primary lesions (3, 4). When Herceptin was used as a first-line therapy in breast cancer patients, metastatic extracranial lesions responded to the agent in 71% of the patients who continued to develop metastatic lesions in the brain (3).

The CNS is protected from the entry of foreign substances by the almost impenetrable blood–brain barrier (BBB) (5, 6), which hampers the delivery of potentially effective diagnostic or therapeutic agents and complicates the treatment of CNS diseases, including malignant brain diseases such as metastatic brain tumors. Because antibody-based agents with a molecular size of ≈150 kDa are easily blocked by the BBB, their delivery to the CNS requires the temporary suspension of the physiological role of the BBB to bar larger molecules from the CNS.

Current advances in acoustic technology have made ultrasound a modality with therapeutic as well as diagnostic applicability. Focused ultrasound techniques facilitate the concentration of acoustic energy on a focal spot, measuring a few millimeters in diameter, and the combined use of MRI permits image-guided target planning and real-time temperature mapping during the sonication of human tumors (7, 8). Not only does ultrasound produce thermal coagulative effects, the combined use of ultrasound and gas bubble-based ultrasound contrast agents induces bioeffects, such as transient changes in cell-membrane permeability (9). Ultrasound has also been shown to be capable of BBB disruption (10), and we have reported that the combination of microbubbles and ultrasound facilitated the reliable disruption of the BBB in rabbits and mice (11–13).

Using a mouse model, we examined the feasibility of delivering Herceptin through the BBB by our technique. We chose mice because in these animals, phase correction is not necessary to produce a focused lesion in the brain through the intact skull (13). We present *in vivo* evidence that the image-defined, site-specific local delivery of Herceptin is possible with our MRI-guided focused ultrasound BBB disruption method and that its concentration in the target tissue can be monitored indirectly on magnetic resonance (MR) images.

Results

BBB Disruption in Mice by Using MRI-Guided Focused Ultrasound. First, BBB opening by MRI-guided focused ultrasound was evaluated at two different power levels. Using a 0.69-MHz focused ultrasound transducer and the injection of 50 μl of Optison (GE Healthcare), we monitored and confirmed the BBB opening by MRI and by the leakage of trypan blue through the BBB into the brain parenchyma after 0.6- and 0.8-MPa sonication (Fig. 1*B*). Measurement of the MR-intensity change caused by leakage of the MR contrast agent into the brain parenchyma showed that the signal intensity initially tended to increase, reaching a saturation point at a later phase (Fig. 1*C*). Consistent with our previous findings (13), macroscopically, 0.6-MPa sonication produced no tissue hemorrhage (Fig. 1*B*), and 0.8-MPa sonication resulted in small, scattered petechiae around the target.

Localized Delivery of Herceptin Through the Mouse BBB and Monitoring with MRI-Guided Focused Ultrasound. Next, the amount of Herceptin delivered through the BBB with our technique was measured. The amount of Herceptin in unsonicated tissues was below the detection threshold in eight of nine cases; we observed a modest increase (1,032 ng/g of tissue) in only one case. On the other hand, after 0.6- or 0.8-MPa sonication and the injection of 50 μl of Optison, the amount of Herceptin in the target tissue increased to 1,504 and 3,257 ng/g of tissue, respectively. Its concentration was significantly higher in tissues sonicated with 0.8 MPa than 0.6 MPa ($P = 0.004$, Welch test) (Fig. 2*A*). Analysis of the normalized MR-intensity change and the Herceptin concentration in sonicated and unsonicated regions revealed

Conflict of interest statement: No conflicts declared.

Abbreviations: BBB, blood–brain barrier; FSE, fast-spin echo; HE, hematoxylin/eosin; MR, magnetic resonance; ROI, region of interest; VAF, vanadium acid fuchsin.

*To whom correspondence should be addressed. E-mail: kullervo@bwh.harvard.edu.

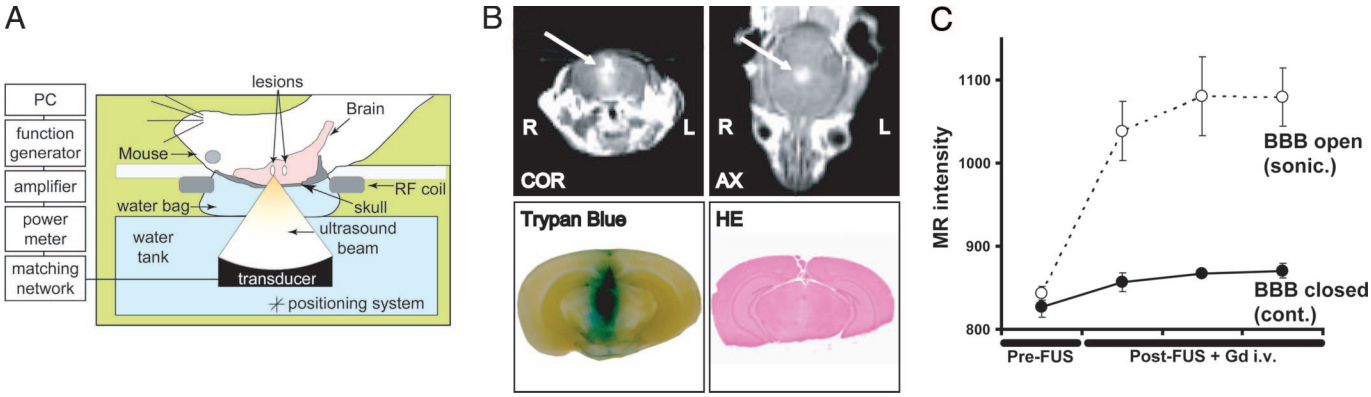

Fig. 1. Experimental settings and BBB disruption in mice by MRI-guided focused ultrasound. (*A*) Diagram and protocol for BBB opening used in this experiment. Mice in the supine position were placed on the sonication table in the MR scanner. The ultrasound beam was focused through the intact skull on the target in the brain. (*B* and *C*) MR monitoring of BBB disruption and photographs of harvested brains showing BBB disruption induced by focused ultrasound. (*B*) Representative example with BBB disruption achieved by 0.6-MPa (peak negative-pressure amplitude) focused ultrasound exposure. (*Upper*) The BBB opening was easily monitored by leakage of the MR contrast agent into the brain parenchyma on axial (AX) and coronal (COR) MR images (arrows). (*Lower Left*) The location of the BBB opening was confirmed by trypan blue staining of the affected area. (*Lower Right*) No apparent macroscopic damage related to BBB disruption can be seen. (*C*) Magnitude of BBB disruption in the animal presented in *B* monitored by the MR-intensity change. Absolute values of the MR intensity of the sonicated target (○) and the contralateral side (control; ●) are plotted for repeated image acquisitions after sonication. Data are presented as the mean ± SD of four voxels.

that the values exhibited a good correlation ($R = 0.59$ for 1.5 T and $R = 0.77$ for 3.0 T) (Fig. 2*B*).

Histological Evaluation After Focused Ultrasound-Induced BBB Disruption in Mice. We carefully assessed the damage from focused ultrasound-induced BBB disruption. When BBB disruption was by 0.6-MPa sonication, only a few scattered extravasated red blood cells were observed. Although 0.8-MPa sonication did not result in serious damage, the number and size of extravasations increased (Fig. 3*A* and Table 1). After 0.8-MPa sonication, there were a few TUNEL-positive apoptotic cells at sites of the most severe extravasation (Fig. 3*B* and Table 1); their number was greater than after 0.6-MPa sonication. VAF staining showed that neither 0.8- nor 0.6-MPa sonication resulted in major ischemic changes.

Discussion

Among currently available molecular targeting drugs, the antibody-based chemotherapeutic agent Herceptin, an anti-HER2 mAb, has proven remarkably effective in the local and distal control of human breast cancer lesions (1, 14). Rituxan (ritux-

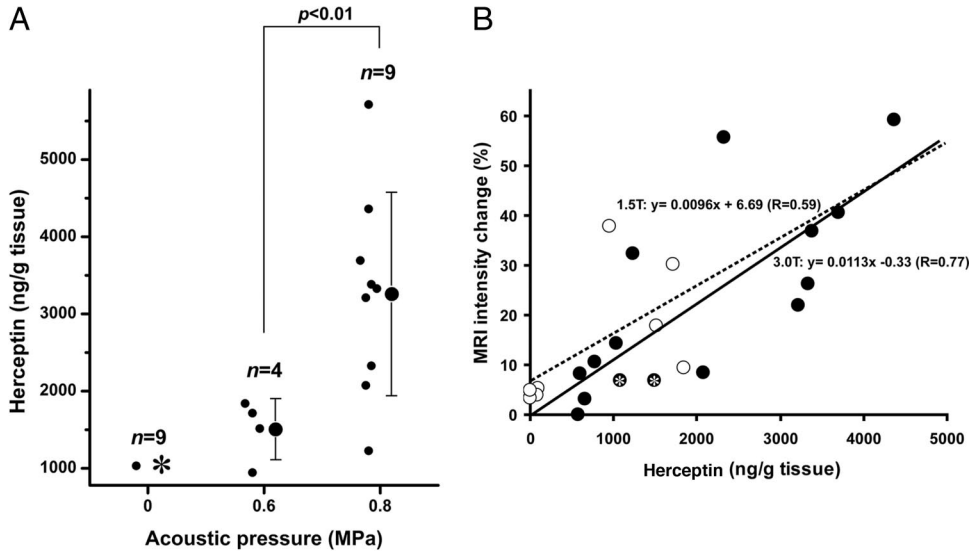

Fig. 2. Delivery of Herceptin into mice brain by MRI-guided focused ultrasound-induced BBB disruption. (*A*) Herceptin concentration in sonicated tissues after focused ultrasound-induced BBB disruption. The concentrations of Herceptin in the sonicated or control tissues are plotted as a function of the applied acoustic pressure. Raw data (●) and the mean ± SD are shown. In the control (0 MPa), Herceptin was below the lower limit of the detection range (780 ng/g of tissue) in eight of nine cases (asterisk). The concentration of Herceptin in the sonicated tissue increased as a function of the applied power [0.6 vs. 0.8 MPa: $P = 0.004$ (Welch test)]. (*B*) Correlation between tissue Herceptin concentration and MR-intensity changes after BBB opening induced by focused ultrasound. The MR-intensity changes as a function of the tissue Herceptin concentration are plotted. Data obtained with the 3.0-T and 1.5-T MRI scanner are plotted as ● and ○, respectively. Data points with a Herceptin concentration below the detection limit (780 ng/g of tissue) represent estimated values calculated from the A_{405} by using the Easy-Titer Human IgG (H+L) assay kit. The MR intensity and Herceptin concentration showed a good correlation ($R = 0.59$ for 1.5 T and $R = 0.77$ for 3.0 T). Two asterisked data are not included for analysis in *A* because an i.v. catheter problem made the injection of Optison unsuccessful, which affects the BBB opening by ultrasound.

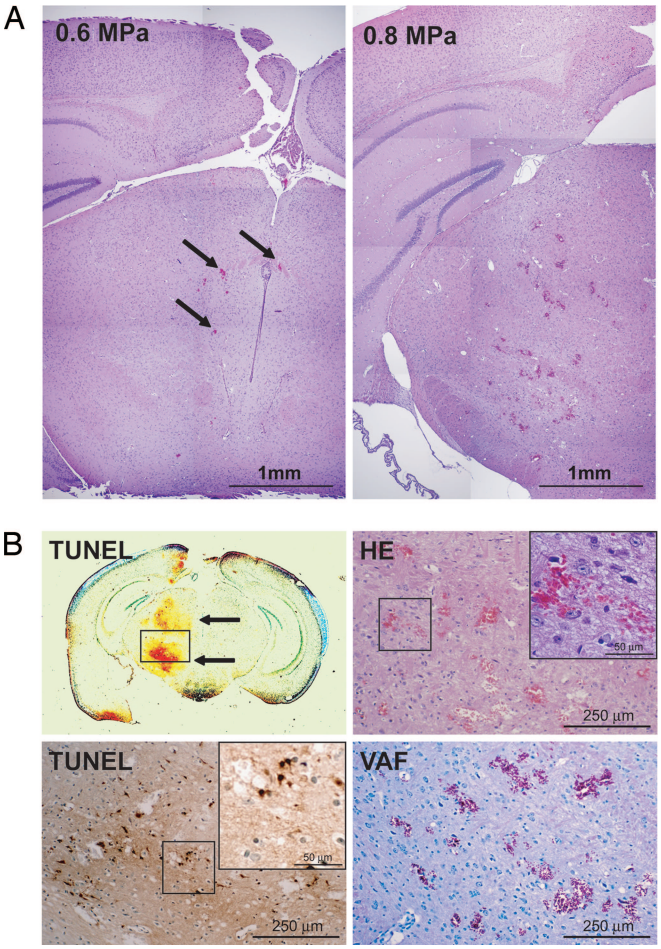

Fig. 3. Impact of focused ultrasound-induced BBB disruption on tissues. (*A*) Microscopic overview of a mouse brain subjected to focused ultrasound-induced BBB disruption. (*Left*) Hematoxylin/eosin (HE)-stained tissue from the mouse shown in Fig. 1. Sonication was with an acoustic pressure of 0.6 MPa. Except for a few extravasations (arrows), no major damage can be seen. (*Right*) HE-stained tissue from a mouse sonicated with 0.8 MPa. Although there are more and larger extravasations, tissue integrity is retained. (*B*) Magnified view of HE, TUNEL, and vanadium acid fuchsin (VAF) staining of the brain of a mouse subjected to 0.8-MPa sonication. TUNEL-positive cells are concentrated at sites with the most severe extravasation (*Left Upper* and *Lower*). Examination of ischemic tissue changes by VAF staining (*Right Lower*) revealed no major ischemic changes (acidophilic cells) even around the most severe extravasations (*Right Upper*).

imab), an anti-CD20 mAb, has also been shown to be effective in patients with lymphoma (15), and there is accumulating evidence that antibodies against amyloid β can reverse cognitive deficits in early Alzheimer disease (16, 17).

The use of these antibody-based agents in the CNS raises a major and difficult problem. Because the CNS is protected from exogenous substances by the BBB, antibodies with a molecular size of 150 kDa are easily blocked. When Herceptin or Rituxan was administered by systemic injection, the cerebrospinal fluid level of either agent was only 0.3% or 0.1% of that in the serum (18, 19). In addition, the use of Herceptin to treat breast cancer patients has led to an increase in the incidence of brain metastasis (3, 4), which can develop even though extracranial lesions continue to respond to Herceptin (3).

Several methods have been proposed to circumvent the BBB for drug delivery. For the delivery of TF-CRM107, a transferrin receptor ligand-targeted toxin conjugate, to the target location in patients with malignant gliomas, a method called ''convection'' was used (20); a catheter inserted into the brain or tumor provided the route for drug administration. In rats, the intracerebral microinfusion of Herceptin was effective in curing intracerebral metastatic breast tumors (21), and the injection of hypertonic solutions into the carotid artery produced a temporary opening of the BBB in humans (22). Although these techniques are appealing, they involve invasive procedures, and thus they limit the number of treatment-eligible candidates. Other methods have focused on modifying the agents to allow their penetration of the BBB (5, 23, 24), but these methods cannot provide site specificity. Moreover, rendering antibodies able to penetrate the BBB continues to be a challenge.

Table 1. Quantification of tissue damage

Acoustic pressure (calibrated in water), MPa	No. of microhemorrhages	No. of TUNEL-positive cells
0.6 ($n = 3$)	25 ± 8.18	11.6 ± 9.45
0.8 ($n = 2$)	77 ± 4.24	28 ± 22.62

The number of sites exhibiting microhemorrhages and TUNEL-positive cells was counted under a microscope in sections with the most severe damage. Data are the mean ± SD.

We previously demonstrated that focused ultrasound-induced BBB disruption made it possible to deliver a dopamine D_4 receptor-targeting antibody across the mouse BBB (13) and that the ultrasound parameters we used here did not produce macroscopic tissue damage in rabbits and mice subjected to BBB opening (11, 13). Because the ultrasound energy is concentrated only around the target area, therapeutic agents can be delivered site-specifically, sparing the surrounding tissue. Compared with catheter insertion into the brain, the histological damage attributable to focused ultrasound BBB disruption (Fig. 3 *A* and *B*) seemed to be within an acceptable range. Our previous study revealed that focused ultrasound-induced BBB disruption produced neither long-term nor delayed damage in the rabbit brain (12). The Herceptin concentration in mouse brain tissue showed a good correlation with the measured MR-intensity change after opening the BBB (Fig. 2*B*), indicating that our integrated MRI system returns excellent feedback information to the operator. Because this focused ultrasound-induced BBB disruption has been shown to be transient and reversible (11), it is reasonable to assume that multiple or repeated use of this technique is possible in the clinical setting.

The enhanced, active transport of molecules across the BBB after sonication suggests the involvement of a biophysiological effect created by the microbubbles and ultrasound (11). Our previous studies showed that in rabbits subjected to 1.63-MHz sonication for BBB opening, the temperature elevation in the targeted tissues was only 0.025°C for consistent BBB opening. Thus, it is unlikely that temperature elevation was a significant contributor to BBB leakage (25). When acoustic emissions from the area sonicated for BBB opening were measured, BBB disruption was achieved even under conditions where no wideband emission was detected (26). Because wideband emission is considered to be a signature for inertial cavitation (27), the oscillation rather than the collapse of microbubbles in capillary vessels appears to be the key factor for BBB opening (26). It should be noted that the presence of microbubbles is necessary for consistent BBB opening; in their absence, we observed only modest BBB disruption in rabbits even under high-pressure amplitudes (25).

We have previously demonstrated that ultrasound-wave distortions attributable to the skull can be corrected and that ultrasound of therapeutic intensity can be focused through the intact human skull by using ultrasound transducers arranged in

Table 2. MRI parameters used in the study

Sequence	Field strength, T	TR, ms	TE, ms	Matrix	Echo train length	Flip angle, °	Bandwidth, kHz	No. of acquisitions	Field of view/slice thickness, mm
FSE T1-W*									
	1.5	500	14	256 × 256	4	90	16	4	100/1.5
	3.0	500	16	256 × 256	4	90	16	4	80/1.5
Gradient-echo†									
	1.5	8.2	2	256 × 128	NA	30	32	1	100/3
	3.0	12.8	2	256 × 128	NA	30	32	1	100/3

TR, repetition time; TE, echo time; FSE T1-W, fast-spin echo T1-weighted sequence; NA, not applicable.
*Purposes: target selection and contrast enhancement.
†Purpose: tissue anatomy targeting.

a phase-array configuration (28). The current study suggests the possibility of using our focused ultrasound-induced BBB disruption technique in the clinical setting. The power level required for BBB opening in rabbits and mice is not different (11, 13). Therefore, we postulate that different species do not necessitate large modifications in the ultrasound parameters for BBB opening. We suggest that in humans, it may be possible to achieve BBB opening through the intact skull by using a phased-array focused ultrasound transducer (28) and ultrasound parameters similar to those used here.

In conclusion, the data presented here suggest that our MRI-guided focused ultrasound-induced BBB disruption method is a promising technique for the delivery of large molecular agents, including antibody-based cancer therapeutic agents, to the CNS. The ability to deliver antibody directly to the CNS may be a large step forward in the treatment of patients with of CNS malignancies.

Materials and Methods

Ultrasound Equipment. The ultrasound fields were generated with a focused, piezoelectric transducer manufactured in-house; its diameter is 100 mm, the radius of curvature is 80 mm, and the resonant frequency is 0.69 MHz. The −6-dB beam width and axial focal length of the produced focal spot were 2.3 mm and 14 mm, respectively. The transducer-driving equipment was similar to that reported in ref. 29. Sonication was pulsed with a burst length of 10 ms and a repetition frequency of 1 Hz (duty cycle, 1%). The total sonication duration was 40 s. Peak negative-pressure amplitude levels were kept constant over the duration of each sonication. We used 0.6 or 0.8 MPa (peak negative-pressure amplitude calibrated in water), depending on the experiments. These values were chosen based on earlier findings that the ultrasound parameters used here did not produce macroscopic tissue damage in mice subjected to BBB opening (13). The acoustic-power output and the focal-pressure amplitude as a function of the applied radiofrequency power were measured as described in ref. 29. Because the ultrasound energy is attenuated during transskull delivery, the actual acoustic pressure in the mouse brain can be expected to be lower. Considering energy attenuation by the skull, the *in situ* pressure at the focus of the mouse brain is estimated to be 87 ± 7% of that measured in water. This value was obtained by measuring the insertion loss of the acoustic pressure by six different skulls in three different locations with a needle hydrophone. The estimated *in situ* spatial-peak temporal-peak intensity (I_{SPTP}) and spatial-peak temporal-average intensity (I_{SPTA}) of each sonication are estimated to be 8.6 and 0.086 W/cm^2, respectively, for 0.6-MPa sonication and 15.2 and 0.152 W/cm^2, respectively, for 0.8-MPa sonication.

Animal Preparation. All of the procedures used in the animal experiments were approved by the Institutional Animal Committee. We used 10-week-old Swiss–Webster mice weighing 30–35 g. They were anesthetized with a mixture of xylazine (10 mg/kg) and ketamine (70 mg/kg). A catheter for injection was placed in the tail vein, the hairs over the skull were removed, and the animal was placed in a supine position on the sonication table (Fig. 1*A*).

Sonication. The animals were prepared as described above and placed on the system. T1-weighted images were obtained to aid in the selection of target locations in the brain. After injecting 20 mg/kg Herceptin into a tail vein, sonication was performed; a 50-μl bolus of the microbubble-based ultrasound contrast agent Optison was injected simultaneously. The agent contains 5–8 × 10^8 albumin-coated microbubbles per ml; the mean diameter of the bubbles is 2.0–4.5 × 10^{-6} m. The brain was sonicated from the dorsal surface into the right hemisphere at a depth of ≈2–3 mm. Because the mouse brain measures ≈5–6 mm along the axis of the ultrasound beam path, the skull base was also sonicated during the procedure. After the sonication procedure and the acquisition of MR images were completed, trypan blue (80 mg/kg) was injected through the tail vein to mark and confirm the site of BBB disruption on tissue blocks.

MRI. We used two different systems to evaluate the feasibility of our technique. The MRI scanner was either a standard 1.5-T or a 3.0-T Signa system (General Electric Medical Systems, Milwaukee, WI). A 7.5-cm-diameter surface coil was placed under the head of each mouse, and sonications were performed through the hole in the coil that was filled with a plastic bag [poly(vinyl chloride), thickness <15 μm] containing degassed water (P_{O_2} <1 ppm) (Fig. 1*A*). The dorsal surface of the head was in direct contact with the degassed water in the plastic bag. A gradient-echo sequence was used to aim the beam at the brain. After obtaining the anatomical orientation of the brain with the gradient-echo sequence, T1-weighted fast-spin echo (FSE) images were acquired at a plane that included the target for sonication. After sonication, T1-weighted FSE images were obtained again and repeated after the injection of a 10-μl i.v. bolus of gadopentetate dimeglumine MR contrast agent (Magnevist; Berlex Laboratories, Cedar Knolls, NJ) to detect and evaluate the opening of the BBB. MR contrast agents were injected ≈10–15 s after the completion of sonication followed by acquisition of T1-weighted FSE images, and their leakage into the brain was monitored to confirm BBB disruption on T1-weighted FSE images. The baseline enhancement on the unsonicated contralateral side served as the control for the integrity of the undisrupted BBB (Fig. 1*C*). The parameters for the MRI scans are listed in Table 2.

Signal Analysis. MRI contrast enhancement was evaluated at each target location by averaging the signal intensity at the selected region of interest (ROI). The signal was normalized to the baseline value in the ROI before contrast injection. ROIs contralateral to the sonicated brain tissue served as the controls.

Tissue Preparation and Histological Examination. Animals were killed ≈4 h after sonication. The choice of this interval was based on our previous findings in mouse brains injected with anti-dopamine D_4 receptor antibodies (13). The brains were immediately removed and fixed in 10% buffered neutral formalin. After substantial fixation of the tissue, tissue blocks that included the sonicated area were embedded in paraffin. In all cases, sonication spots were easily identified by trypan blue (Fig. 1*B*). Serial sections parallel to the beam direction were cut, and every fifth section was stained with HE for histological examination.

Because vascular injury can induce microischemic events and result in ischemic neuronal injury (30), we used staining to detect apoptotic cells and ischemic neurons in adjacent sections on the focal plane. The apoptotic staining method used in this study was described previously by Gavrieli *et al.* (31). TUNEL staining (ApoptTag kit; Intergen, Purchase, NY) was used for the detection of DNA fragmentation and apoptotic bodies in the cells. The sections were counterstained with 0.5% methyl green. To visualize ischemic neurons in the sonicated areas, we used VAF staining and toluidine blue counterstaining (32).

Herceptin Detection and Quantification. Herceptin in the tissue was quantified by measuring the amount of human IgG in the tissue. Because Herceptin is a humanized mAb, the amount of human IgG detected in the mouse brain tissue specimens can be considered to reflect the amount of Herceptin in the tissues.

The mice were killed 4 h after sonication, and their brains were removed immediately. Sonication spots, easily detected by trypan blue staining, were harvested. Tissues on the contralateral side of the brain were harvested as controls. The tissues were homogenized, and the soluble protein fraction was obtained by the slightly modified method of Gearhart *et al.* (33). Tissues were homogenized in 10 vol (e.g., ≈10 ml of buffer per g of tissue) of supplemented modified radioimmunoprecipitation buffer (pH 8.0), which contained 150 mM NaCl, 1% (vol/vol) Nonidet P-40, 0.5% (wt/vol) sodium deoxycholate, 0.1% (wt/vol) SDS, 50 mM Tris, and 10% (vol/vol) glycerol (all from Sigma–Aldrich) and was supplemented with 200 μl of PMSF, 100 μl of protease inhibitor mixture, and 200 μl each of phosphatase inhibitor mixtures 1 and 2 (all from Sigma–Aldrich) per 10 ml of ice-cold buffer. Homogenized tissue samples were placed on a platform rocker (4°C for 1 h), and then supernatant fractions were prepared by centrifugation at ≈14,000 × *g* for 30 min at 4°C.

The amount of human IgG in the samples was quantified by using the Easy-Titer Human IgG (H+L) assay kit (Pierce). As specified by the manufacturer, absorbance at 405 nm (A_{405}) was measured with an MTP-120 microplate reader (Corona Electric, Ibaragi, Japan) and converted to the Herceptin concentration by using a serial dilution of Herceptin as a standard (Fig. 4, which is published as supporting information on the PNAS web site). The minimum detectable amount of Herceptin was 780 ng/g of tissue. The reported <780 ng/g is an estimated value calculated from the obtained A_{405}.

We thank Yong-Zhi Zhang and Sue Agabian for technical assistance in this investigation. This work was supported by the Shinya International Exchange Fund, the Osaka Medical Research Foundation for Incurable Diseases, the Osaka Neurological Institute (M.K.), and National Institutes of Health Grants EB003268 (to K.H.) and U41-RR 019703 (to F.A.J.).

1. Baselga, J. (2000) *Semin. Oncol.* **27,** 20–26.
2. Markesbery, W. R., Brooks, W. H., Gupta, G. D. & Young, A. B. (1978) *Arch. Neurol.* **35,** 754–756.
3. Bendell, J. C., Domchek, S. M., Burstein, H. J., Harris, L., Younger, J., Kuter, I., Bunnell, C., Rue, M., Gelman, R. & Winer, E. (2003) *Cancer* **97,** 2972–2977.
4. Clayton, A. J., Danson, S., Jolly, S., Ryder, W. D., Burt, P. A., Stewart, A. L., Wilkinson, P. M., Welch, R. S., Magee, B., Wilson, G., *et al.* (2004) *Br. J. Cancer* **91,** 639–643.
5. Pardridge, W. M. (2002) *Neuron* **36,** 555–558.
6. Abbott, N. J. & Romero, I. A. (1996) *Mol. Med. Today* **2,** 106–113.
7. Tempany, C. M., Stewart, E. A., McDannold, N., Quade, B. J., Jolesz, F. A. & Hynynen, K. (2003) *Radiology* **226,** 897–905.
8. Hynynen, K., Pomeroy, O., Smith, D. N., Huber, P. E., McDannold, N. J., Kettenbach, J., Baum, J., Singer, S. & Jolesz, F. A. (2001) *Radiology* **219,** 176–185.
9. Kinoshita, M. & Hynynen, K. (2005) *Biochem. Biophys. Res. Commun.* **335,** 393–399.
10. Patrick, J. T., Nolting, M. N., Goss, S. A., Dines, K. A., Clendenon, J. L., Rea, M. A. & Heimburger, R. F. (1990) *Adv. Exp. Med. Biol.* **267,** 369–381.
11. Hynynen, K., McDannold, N., Sheikov, N. A., Jolesz, F. A. & Vykhodtseva, N. (2005) *NeuroImage* **24,** 12–20.
12. McDannold, N., Vykhodtseva, N., Raymond, S., Jolesz, F. A. & Hynynen, K. (2005) *Ultrasound Med. Biol.* **31,** 1527–1537.
13. Kinoshita, M., McDannold, N., Jolesz, F. A. & Hynynen, K. (2006) *Biochem. Biophys. Res. Commun.* **340,** 1085–1090.
14. Bell, R. (2002) *Oncology* **63,** Suppl. 1, 39–46.
15. Maloney, D. G. & Press, O. W. (1998) *Oncology (Williston Park, N.Y.)* **12,** Suppl. 8, 63–76.
16. Janus, C., Pearson, J., McLaurin, J., Mathews, P. M., Jiang, Y., Schmidt, S. D., Chishti, M. A., Horne, P., Heslin, D., French, J., *et al.* (2000) *Nature* **408,** 979–982.
17. Klyubin, I., Walsh, D. M., Lemere, C. A., Cullen, W. K., Shankar, G. M., Betts, V., Spooner, E. T., Jiang, L., Anwyl, R., Selkoe, D. J. & Rowan, M. J. (2005) *Nat. Med.* **11,** 556–561.
18. Pestalozzi, B. C. & Brignoli, S. (2000) *J. Clin. Oncol.* **18,** 2349–2351.
19. Rubenstein, J. L., Combs, D., Rosenberg, J., Levy, A., McDermott, M., Damon, L., Ignoffo, R., Aldape, K., Shen, A., Lee, D., *et al.* (2003) *Blood* **101,** 466–468.
20. Laske, D. W., Youle, R. J. & Oldfield, E. H. (1997) *Nat. Med.* **3,** 1362–1368.
21. Grossi, P. M., Ochiai, H., Archer, G. E., McLendon, R. E., Zalutsky, M. R., Friedman, A. H., Friedman, H. S., Bigner, D. D. & Sampson, J. H. (2003) *Clin. Cancer Res.* **9,** 5514–5520.
22. Doolittle, N. D., Miner, M. E., Hall, W. A., Siegal, T., Jerome, E., Osztie, E., McAllister, L. D., Bubalo, J. S., Kraemer, D. F., Fortin, D., *et al.* (2000) *Cancer* **88,** 637–647.
23. Pardridge, W. M. (2003) *Curr. Opin. Drug Discov. Dev.* **6,** 683–691.
24. Schwarze, S. R., Ho, A., Vocero-Akbani, A. & Dowdy, S. F. (1999) *Science* **285,** 1569–1572.
25. Hynynen, K., McDannold, N., Vykhodtseva, N. & Jolesz, F. A. (2001) *Radiology* **220,** 640–646.
26. McDannold, N., Vykhodtseva, N. & Hynynen, K. (2006) *Phys. Med. Biol.* **51,** 793–807.
27. Lele, P. (1987) in *Ultrasound: Medical Applications, Biological Effects, and Hazard Potential*, eds. Repacholi, M., Grondolfo, M. & Rindi, A. (Plenum, New York), pp. 275–306.
28. Hynynen, K., Clement, G. T., McDannold, N., Vykhodtseva, N., King, R., White, P. J., Vitek, S. & Jolesz, F. A. (2004) *Magn. Reson. Med.* **52,** 100–107.
29. Hynynen, K., Vykhodtseva, N. I., Chung, A. H., Sorrentino, V., Colucci, V. & Jolesz, F. A. (1997) *Radiology* **204,** 247–253.
30. Charriaut-Marlangue, C., Margaill, I., Represa, A., Popovici, T., Plotkine, M. & Ben-Ari, Y. (1996) *J. Cereb. Blood Flow Metab.* **16,** 186–194.
31. Gavrieli, Y., Sherman, Y. & Ben-Sasson, S. A. (1992) *J. Cell Biol.* **119,** 493–501.
32. Victorov, I. V., Prass, K. & Dirnagl, U. (2000) *Brain Res. Brain Res. Protoc.* **5,** 135–139.
33. Gearhart, D. A., Middlemore, M. L. & Terry, A. V. (2005) *J. Neurosci. Methods* **150,** 159–173.